IIETA International Information and Engineering Technology Association
Advancing the World of Information and Engineering

Revue des Composites et des Matériaux Avancés-Journal of Composite and Advanced Materials
Vol. 35, No. 4, August, 2025, pp. 779-790
Journal homepage: http://iieta.org/journals/rcma

A Study on the Use of Heterocyclic Compounds for Surface Protection in Acidic Environments

Asawer S. Temma*, Hanan M. Ali

Department of Chemistry, College of Education for Pure Sciences, University of Basrah, Basrah, Iraq

Corresponding Author Email: asawer.tema@uobasrah.edu.iq

https://doi.org/10.18280/rcma.350420

Received: 15 July 2025
Revised: 16 August 2025
Accepted: 25 August 2025
Available online: 31 August 2025

Keywords:
corrosion inhibition, carbon steel N80, thiazolidine derivatives, SEM, electrochemical

ABSTRACT

This study aims to assess the potential of two synthesized thiazolidine derivatives (AS_3) and (AS_4) in the capacity of preventing corrosion on N80 alloy steel in 1M hydrochloric acid medium. The electrochemical behavior, adsorption isotherms, activation energy, and surface morphology were analyzed using Tafel polarization curves, Langmuir adsorption model, Arrhenius equation, and scanning electron microscope (SEM) coupled with energy-dispersive spectroscopy (EDS) techniques. The findings indicate that both compounds function as efficient mixed-type inhibitors, with inhibition efficiency improving proportionally to inhibitor concentration but exhibiting a slight reduction at higher temperatures. This thermal sensitivity points to a predominant physisorption mechanism in the initial adsorption stages. SEM/EDS results confirmed the formation of a compact, protective surface film, validating the adsorption-driven protection mechanism. The significance of this study lies in the growing demand for environmentally safer and economically viable inhibitors for industrial applications involving acid-induced corrosion, especially in oil and gas applications where N80 carbon steel is widely used. Thiazolidine derivatives show strong affinity for steel surfaces, highlighting their suitability, due to their heteroatoms and π-electron system, offer promising coordination ability with metal surfaces. Thus, AS_3 and AS_4 represent valuable candidates for mitigating acid-induced corrosion, contributing to extended equipment life and reduced maintenance costs in aggressive environments.

1. INTRODUCTION

Corrosion can be described as a process that occurs naturally or through chemical action by which a metal is transformed into a more stable state [1]. However, it incurs significant economic losses worldwide [2]. Most pure forms of metals and alloys are very reactive and readily degrade due to their susceptibility to corrosion resulting from reactions with environmental components [3, 4]. Research into the corrosion inhibition behavior of carbon steel is one of the most common areas of investigation, partly due to its relatively high mechanical strength, affordability, and broad industrial applications. However, carbon steel is also easily corroded. Iron, being a highly reactive material, undergoes frequent corrosion during usage across the industry. Especially in the petrochemical and chemical fields, carbon steel is often subjected to highly acidic media, resulting in shortened service life and a higher likelihood of hazardous incidents [5]. In various industrial branches, acidic media are commonly applied to remove unwanted deposits and oxide layers from steel surfaces. These solutions are frequently used to enhance oil and gas extraction by means of acidizing operations within the petroleum sector. Such processes typically lead to significant corrosion in steel pipes, tubes, and equipment [6].

Corrosion is arguably the most common and undesirable phenomenon, representing a natural process that results from electrochemical interactions between metals and corrosive media, leading to their deterioration [7]. Corrosion inhibitors are one of the most efficient strategies for protecting metals from corrosion [8]. Inhibitors are chemical substances utilized to prevent or decrease corrosion on metal surfaces in corrosive conditions [9]. They are considered a key preventive measure against corrosion. The nature and effectiveness of their functional groups and electron density at the donor atoms play a critical role in determining the inhibition efficiency [10, 11]. Thiazolidine derivatives are environmentally friendly molecules with wide applications in the food, pharmaceutical, and biological industries. Thiazolidine derivatives containing additional heteroatoms such as N and O, along with aryl-containing compounds, have been utilized to inhibit the corrosion of metals in various aggressive conditions. The density of electrons of inhibitor molecules due to lone pairs on heteroatoms, oxygen, nitrogen, sulfur, and phosphorus, and π-electrons enhances their interaction with metal surfaces by coordination with vacant d-orbitals. Therefore, the inhibitor forms coordinate covalent bonds with the metal surface. Several factors affect the adsorption capability of the inhibitor to the metal surface, including the surface charge of the metal,

its chemical composition, the type of corrosion medium, and the chemical composition of the inhibitor [12, 13]. Both AS_3 and AS_4 exhibit distinct advantages over previously reported thiazolidine-based corrosion inhibitors. They are synthesized through a straightforward, one-step reaction using inexpensive and non-toxic precursors, offering a more sustainable and cost-effective alternative [14]. Unlike other inhibitors that require complex synthetic pathways or incorporate halogenated frameworks, AS_3 and AS_4 deliver superior inhibition efficiencies exceeding 90% at relatively low concentrations. The presence of functional groups significantly enhances their adsorption affinity, which aligns well with the thermodynamic behavior predicted by the Langmuir isotherm. Moreover, SEM/EDS analyses confirm the formation of a uniform and protective surface layer, underscoring their practical viability as effective corrosion inhibitors in acidic environments [15]. Recent developments in corrosion science have also highlighted the growing interest in environmentally friendly, or "green", corrosion inhibitors. While synthetic organic inhibitors have long dominated the field, emerging research has demonstrated the effectiveness of plant-based extracts as viable alternatives. These natural compounds, often rich in polyphenols and flavonoids, exhibit strong adsorption capabilities on metal surfaces and are capable of forming protective layers comparable to conventional inhibitors. The integration of such approaches reflects a broader shift toward sustainable practices in industrial corrosion control, expanding the available options for efficient and eco-conscious protection strategies [16, 17].

2. MATERIALS AND METHODS

The materials used in this experiment include 4-hydroxybenzaldehyde and 3-hydroxy-4-methoxybenzaldehyde, both sourced from Merck. Other reagents were purchased from Sigma-Aldrich. All chemicals possessed a purity of 99%. In this study, the N80 carbon steel specimens employed were supplied by the South Oil Company (Basra, Iraq). Their chemical composition was verified to conform with the standard specifications for N80-grade steel, with weight percentages composition of the alloy was 0.39% carbon, 0.005% silicon, 0.06% phosphorus, 1.4% manganese, and the remainder iron. Samples were obtained from the same manufacturing lot. FT-IR measurements were carried out on a Shimadzu FT-IR 8400S spectrophotometer with KBr discs in the range of 4000-500 cm^{-1}. ^{1}H-NMR data were acquired using a Bruker 500 MHz spectrometer with tetramethyl silane TMS as the internal standard. The surface features of materials were noticed utilizing a scanning electron microscope (SEM), specifically a TESCAN MIRA 3 FEG-SEM device. Hydrochloric acid was used as the corrosive medium and was diluted with non-ionic water.

2.1 Synthesis of thiazolidine derivatives (AS_3, AS_4)

The thiazolidine derivatives, (4-hydroxyphenyl) thiazolidine-4-carboxylic acid (AS_3) and 2-(3-hydroxy-4-methoxyphenyl) thiazolidine-4-carboxylic acid (AS_4), were synthesized by reacting 0.01 mole of L-cysteine with 0.01 mole of either 4-hydroxybenzaldehyde or 3-hydroxy-4-methoxybenzaldehyde, respectively. The reaction was executed in a 100 mL Erlenmeyer flask containing a blend of 50 mL ethanol and 10 mL water. The mixture was agitated magnetically at 25°C for 12 hours. The resulting solid was filtration, and washed with diethyl ether, and left to dry. The solid was then recrystallized from a 1:3 mixture of water and ethanol, yielding white crystals, Scheme 1 [18].

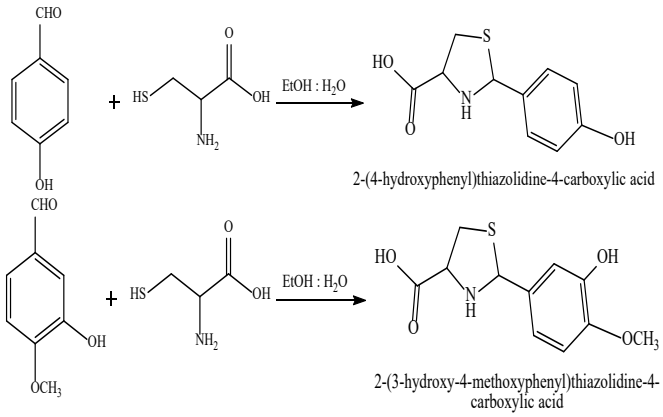

Scheme 1. Preparation steps of Thiazolidine derivatives (AS_3, AS_4)

2.2 Preparation of inhibitor concentrations (AS_3, AS_4)

To evaluate the Tafel polarization behavior of N80 carbon steel, a set of 1 M HCl solution was prepared. 1 M of HCl was selected as the corrosive medium due to its widespread application in industrial acid pickling, oil well acidizing, and scale removal processes. This acid provides a highly reactive and practical environment that effectively dissolves iron oxides while closely simulating harsh real-world conditions. Moreover, the use of a 1 M concentration is well established in the literature for evaluating organic corrosion inhibitors, facilitating meaningful comparisons with related studies [19, 20] with various concentrations of inhibitor AS_3 and AS_4 (0.005, 0.001, 0.0005, and 0.0001 M). Steel specimens (3×2×0.2) cm were immersed in this solution.

3. RESULTS AND DISCUSSION

3.1 Chemistry

The FT-IR spectra (KBr, cm^{-1}) of AS_3 and AS_4 displayed features characteristic of zwitterionic structures, Scheme 2, similar to those found in amino acids. Broad absorption bands were observed in the range of 3390–2500 cm^{-1}, corresponding to secondary amine salt ($+NH_2$), and bands at 1519–1597 and 1429 cm^{-1}, corresponding to carboxylate salt (COO^-) [21].

The spectra also exhibited the disappearance of the SH band around 2600 cm^{-1}, indicating successful synthesis, and the absence of aldehyde C=O bands in the range of 1700–1750 cm^{-1}. Additionally, stretching vibrations of aromatic C–H were observed within the range of 3000–3057 cm^{-1}, and the bands at 2983–2900 cm^{-1} were assigned to aliphatic C–H vibrations. Aromatic C=C stretching modes were detected in the range of 1575–1492 cm^{-1}. Strong bands characteristic of the thiazolidine ring were also observed at 615 cm^{-1} (C-S), 1250–1321 cm^{-1} (C-N), and 1100–1150 cm^{-1} (C-O). An increase in bands between 2500–1900 cm^{-1} indicated hydrogen bonding effects, particularly in the thiazolidine-4-carboxylic acid ring, which influenced OH and NH group vibrations [22]. The 1H-NMR chemical shifts (DMSO-d_6) appeared at 2.5 ppm and 3.3 ppm, with signals at 5.29–5.56

ppm (s, 1H, H–C–S), 3.9–4.21 ppm (t, 2H, H–C–C=O), and 6.9–7.5 ppm (d, 4H, H–Ar). The carboxylic acid proton and NH proton signals were sometimes not visible due to the zwitterionic nature of the compounds [23], Figures 1-4, FT-IR and ^{1}H-NMR spectra of AS_3 and AS_4.

While chromatographic techniques are commonly employed to assess compound purity, this study is aligned with numerous contemporary investigations anticipated functional groups. Moreover, the ^{1}H-NMR spectra showed no extraneous or unexpected signals, indicating the absence of unreacted starting materials or by-products. This approach is widely supported in recent literature, where FT-IR and NMR analyses are routinely utilized to confirm compound purity in lieu of chromatographic data. Collectively, these findings affirm both the successful synthesis and the chemical purity of the prepared molecules [24].

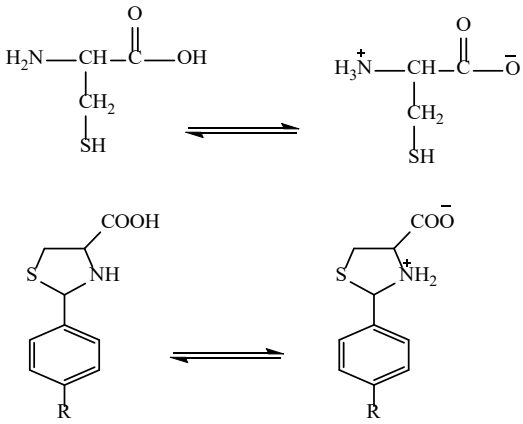

Scheme 2. Zwitterionic structure of the compounds

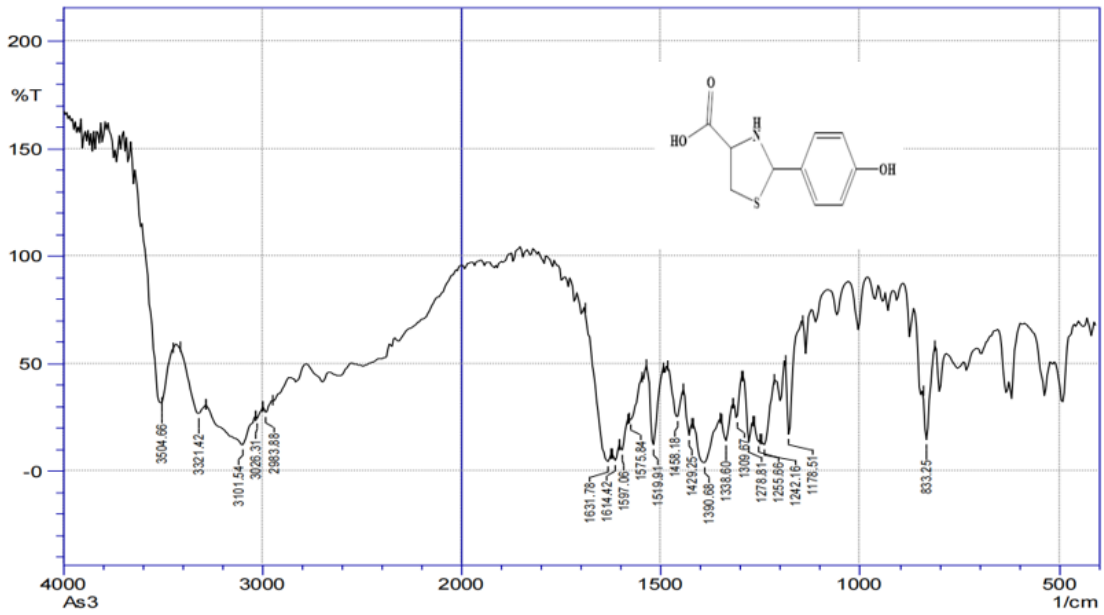

Figure 1. FT-IR spectrum of AS_3

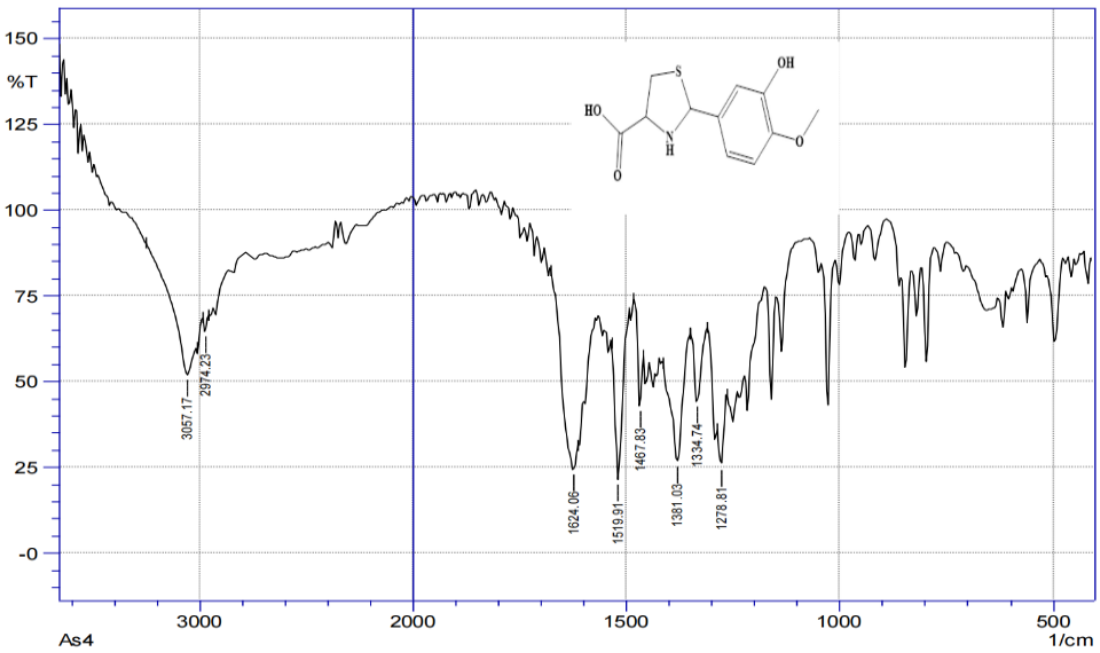

Figure 2. FT-IR spectrum of AS_4

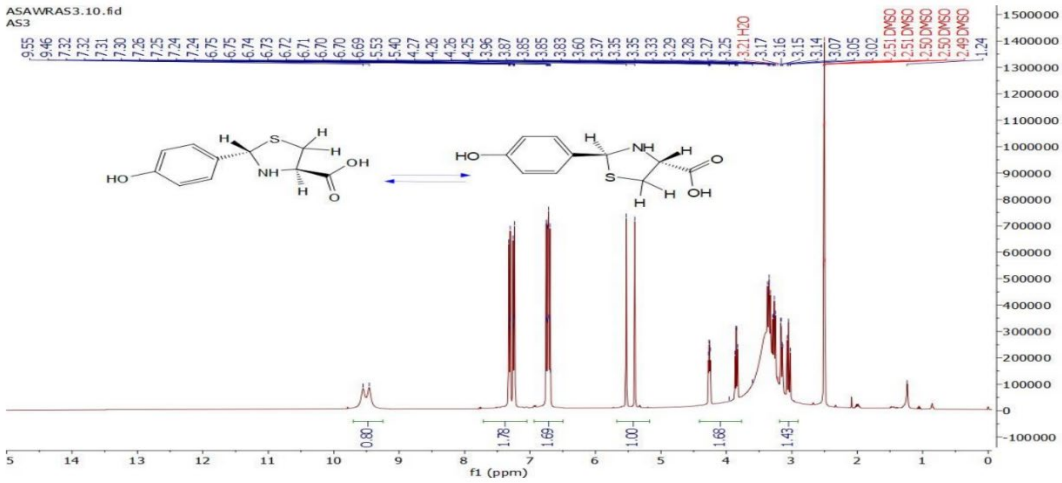

Figure 3. ^{1}HNMR spectrum of AS_3

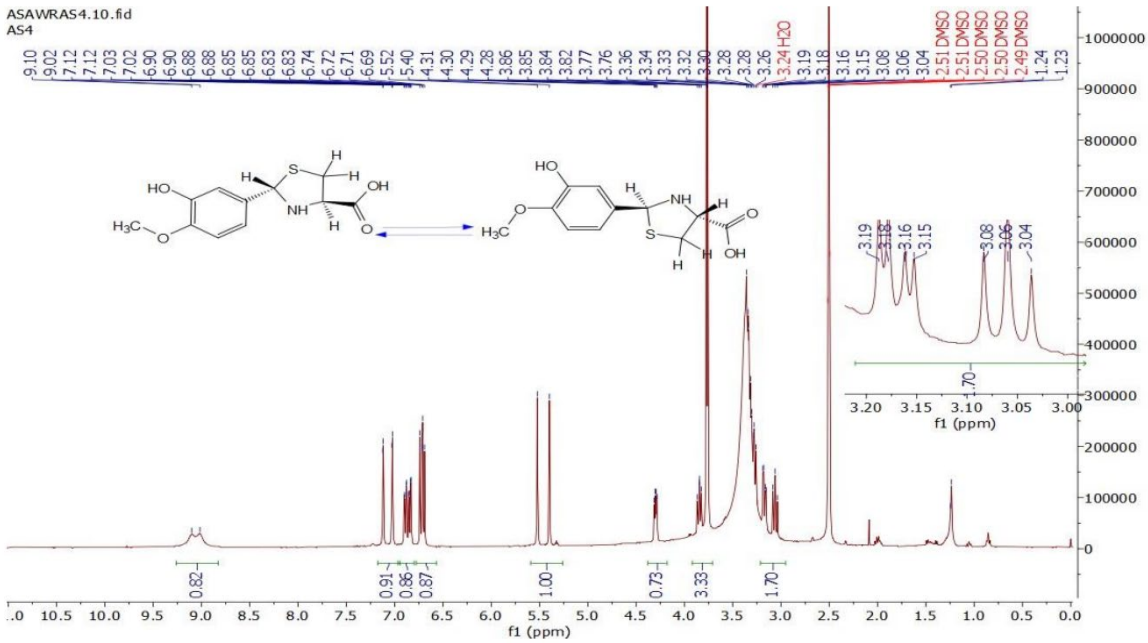

Figure 4. ^{1}H-NMR spectrum of AS_4

3.2 Polarization curves (Tafel plots)

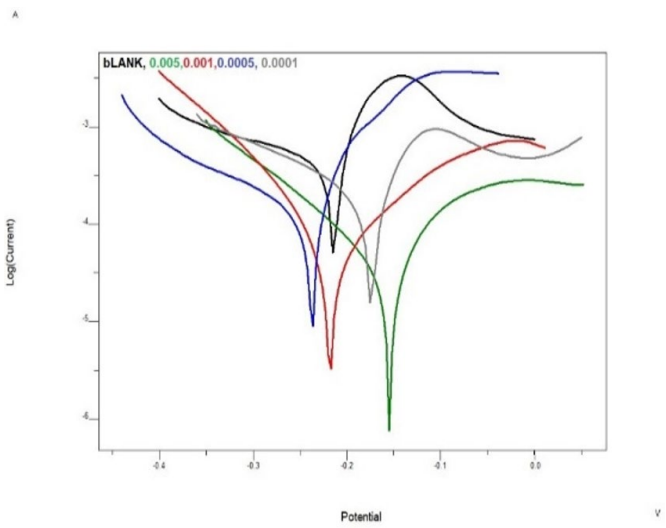

Figure 5. Tafel plot of carbon steel in the presence of AS_3

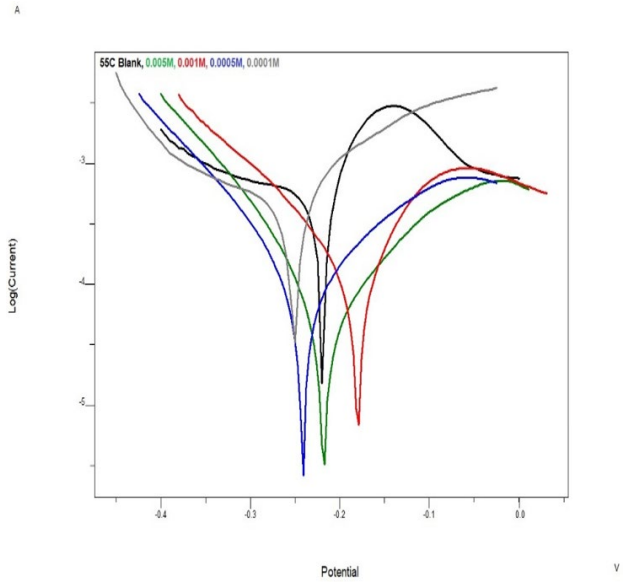

Figure 6. Tafel plot of carbon steel in the presence of AS_4

The polarization behavior of N80 carbon steel was investigated in 1M HCl, both with and without carbon steel in the presence and absence of different concentrations of the inhibitors AS3 and AS4 at various absolute temperatures. Electrochemical measurements were carried out over a potential range of ±400 mV. Figures 5 and 6 illustrate the polarization curves for compounds AS3 and AS4, respectively, at 328 K. As the inhibitor concentration increased, a slight shift in corrosion potential (Ecorr) was observed, moving from more negative values toward the anodic direction. This behavior indicates the creation of a shielding film across the steel surface, thereby decreasing the corrosion current. A displacement in Ecorr greater than 80mv classifies the inhibitor as acting in either an anodic or cathodic manner. Within the research, the shift was within 50 mV, indicating that both AS3 and AS4 function as mixed-type inhibitors. This implies that their addition to the acidic medium hinders anodic reactions and delays hydrogen gas evolution during the cathodic process [25]. Tables 1 and 2 show the variations in the βa and βc parameters as the inhibitor concentration increases, indicating their adsorption on both anodic and cathodic sites [26]. The corrosion reactions occurring in hydrochloric acid solution can be represent as follows:

$$Fe_{(s)}+2HCl_{(aq)} \rightarrow FeCl_{2(aq)}+H_{2(g)}$$

Anodic reaction:

$$Fe \rightarrow Fe^{2+} + 2e^{-}$$

Cathodic reaction:

$$2H^{+} + 2e^{-} \rightarrow H_2\uparrow$$

Table 1. Polarization data of N80 steel with AS_3 at different concentrations and temperatures

Inhibitor Concentration	T (K)	-Ecorr (mV)	Icorr (mA/cm²)	βc (mV/dec)	βa (mV/dec)	CR (mpy)	Surface Coverage Area (θ)	Inhibition Efficiency IE%
Blank	298	211.3	0.18610	275	32	0.084769	-	-
	308	193.7	0.25630	315	63	0.116745	-	-
	318	221.2	0.33020	355	21	0.150406	-	-
	328	214.1	0.40330	345	55	0.183703	-	-
0.005M	298	185.9	0.01332	128	115	0.006067	0.92	92.84
	308	170.3	0.02035	125	124	0.009269	0.92	92.06
	318	175.3	.02876	143	98	0.0131	0.91	91.29
	328	158.3	0.04319	136	117	0.019673	0.89	89.29
0.001M	298	258.0	0.01938	115	51	0.008828	0.89	89.58
	308	168.6	0.02876	137	68	0.0131	0.88	88.77
	318	190.4	0.04868	166	170	0.022174	0.85	85.25
	328	209.7	0.06996	106	147	0.031867	0.82	82.65
0.0005M	298	187.7	0.04566	184	91	0.020798	0.75	75.46
	308	245.8	0.06598	141	31	0.030054	0.74	74.25
	318	206.0	0.08896	176	149	0.040521	0.73	73.05
	328	235.9	0.11395	230	54	0.051904	0.71	71.74
0.0001M	298	232.9	0.10227	232	90	0.046584	0.45	45.05
	308	161.4	0.14370	272	104	0.065455	0.43	43.93
	318	159.4	0.18770	162	88	0.085497	0.43	43.15
	328	169.6	0.23270	280	80	0.105995	0.42	42.30

Table 2. Polarization data of N80 steel with AS_4 at different concentrations and temperatures

Inhibitor Concentration	T (K)	-Ecorr (mV)	Icorr (mA/cm²)	βc (mV/dec)	βa (mV/dec)	CR (mm/y)	CR mpy	Surface Coverage Area (θ)	Inhibition Efficiency IE%
Blank	298	211.3	0.18610	275	32	85.080	0.08476855	-	-
	308	193.7	0.25630	315	63	117.20	0.11674465	-	-
	318	221.2	0.33020	355	21	151.00	0.1504061	-	-
	328	214.1	0.40330	345	55	184.40	0.18370315	-	-
0.005M	298	186.3	0.01231	121	107	5.6072	0.00560721	0.93	93.38
	308	177.8	0.01941	115	137	12.330	0.00884126	0.92	92.43
	318	166.1	0.03925	118	124	17.878	0.01787838	0.88	88.11
	328	213.1	0.05813	93	135	26.478	0.02647822	0.85	85.58
0.001M	298	206.4	0.02549	164	96	11.610	0.0116107	0.86	86.30
	308	179.2	0.04001	112	136	18.224	0.01822456	0.84	84.38
	318	197.8	0.07080	165	121	39.765	0.0322494	0.78	78.55
	328	190.7	0.1130	129	160	51.471	0.0514715	0.71	71.98
0.0005M	298	241.8	0.03423	95	70	15.591	0.01559177	0.81	81.60
	308	192.1	0.0598	159	95	24.897	0.0272389	0.76	76.67
	318	239.1	0.09690	92	73	44.137	0.04413795	0.70	70.65
	328	241.7	0.11900	115	190	54.204	0.0542045	0.70	70.49
0.0001M	298	191.6	0.04218	194	114	23.444	0.01921299	0.77	77.34
	308	182.7	0.08087	161	93	33.324	0.03683629	0.68	68.45
	318	149.2	0.10660	141	153	48.556	0.0485563	0.67	67.71
	328	247.1	0.18070	233	85	82.308	0.08230885	0.55	55.19

As indicated in Tables 1 and 2, the corrosion current density (icorr) is higher in the uninhibited solution, demonstrating extensive metal dissolution and hydrogen evolution, leading to a drop in pH accompanied by a rise in icorr. In contrast, in the presence of the inhibitors, icorr consistently decreases as the inhibitor concentration increases and increases with temperature, suggesting greater protection at higher inhibitor levels and a reduction in efficiency with rising temperature [27].

3.3 Study on corrosion kinetics and inhibition efficiency

Eqs. (1) and (2) were used to calculate the inhibition efficiency (IE%) and surface coverage (θ) from the corrosion current densities [28, 29]:

$$IE\% = [i_{corr.uninh} - i_{corr.inh} / i_{corr.uninh}] \times 100 \quad (1)$$

$$\theta = [i_{corr.uninh} - i_{corr.inh} / i_{corr.uninh}] \quad (2)$$

From the data, both IE% and θ increased with rising inhibitor concentrations at each temperature, attributed to the formation of a protective layer on the alloy surface. This layer increases in thickness with inhibitor concentration, enhancing protection [30]. However, inhibition efficiency decreased at higher temperatures, likely due to desorption of the physically adsorbed layer, consistent with a physisorption mechanism in the early stages followed by chemisorption [31]. Figure 7 and Figure 8 show the relationship between inhibition efficiency (IE%) and temperature for different concentrations of AS_3 and AS_4, respectively. The corrosion rate (CR) is relatively high in the absence of inhibitors, which can be ascribed to rapid metal dissolution. The addition of inhibitors at higher concentrations reduces CR and increases IE% [32].

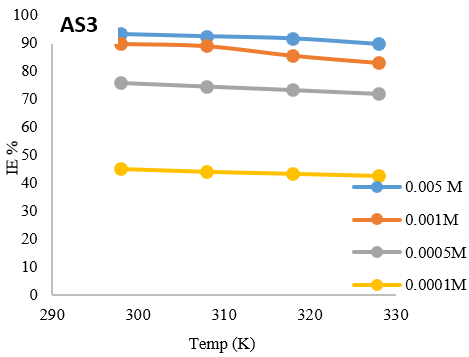

Figure 7. Effect of temperature on IE% at various concentrations of AS_3

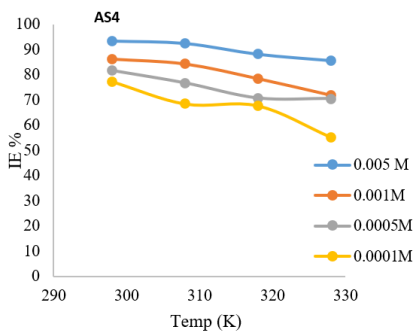

Figure 8. Effect of temperature on IE% at various concentrations of AS_4

Surface coverage θ at different inhibitor concentration was determined using the Tafel extrapolation method to gain insight into the adsorption behavior and the mechanisms of inhibition on N80 carbon steel. Organic inhibitors adhere to the metal surface by replacing previously adsorbed water molecules, as illustrated in (Eq. (3)).

$$Org_{(solu)} + \chi H_2O_{(ads)} \rightarrow Org_{(ads)} + \chi H_2O_{(solu)}$$

Adsorption isotherms, particularly the Langmuir model (Eq. (3)), offer key aspects of how the inhibitor adsorbs onto the metal surface [33].

$$C/\theta = 1/K_{ads} + C \quad (3)$$

In this equation, C stands for the inhibitor concentration, θ is the degree of surface coverage, and K_{ads} is the equilibrium constant of adsorption. Figure 9 and Figure 10 display the Langmuir plots for AS_3 and AS_4 at various temperatures, showing a proportional relationship between C/θ and C with strong correlation coefficients ($R^2 \approx 0.99$), confirming Langmuir-type adsorption behavior. This suggests uniform adsorption without interactions among adsorbed molecules.

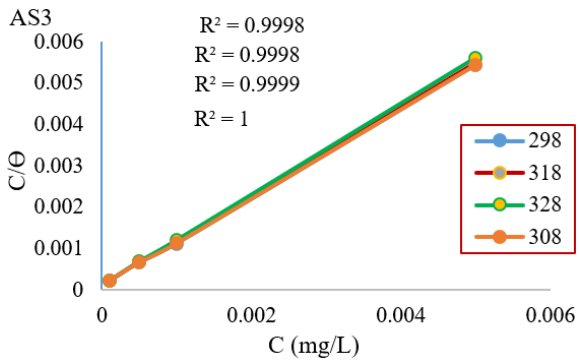

Figure 9. Langmuir adsorption isotherms (AS_3)

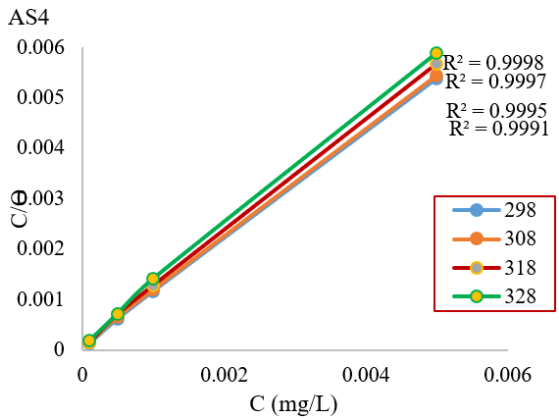

Figure 10. Langmuir adsorption isotherms (AS_4)

$\Delta G°_{ads}$ (standard free energy of adsorption) was determined using Eq. (4):

$$\Delta G°_{ads} = -RT \ln(55.5 \times K_{ads}) \quad (4)$$

In this equation, R denotes the universal gas constant, T is the absolute temperature in kelvin, K is the adsorption equilibrium constant. The constant 55.5 corresponds to the molar concentration of water. According to Table 3, the

negative Gibbs free energy ΔG° adsorption readings validate the spontaneous nature of the adsorption process. The p-values associated with the linear regression analyses for AS_3 and AS_4 were computed across the four investigated temperatures (298, 308, 318, and 328 K). In every case, the coefficient of determination (R^2) exceeded 0.999, demonstrating an exceptional fit to the model. More importantly, the regression slope p-values were consistently found to be below 0.01, indicating strong statistical significance ($p < 0.01$) and effectively ruling out the likelihood of random correlation. These outcomes provide compelling evidence that the Langmuir adsorption isotherm reliably characterizes the adsorption behavior of both compounds on carbon steel N80 in acidic media [34, 35].

Table 3. Langmuir isotherm data for AS_3 and AS_4 adsorption on carbon steel at various temperatures

Comp.	Δ H_{ads} (kJ.mol^{-1})	Temperature K	R^2	P-Value	K_{ads}	Log K_{ads}	ΔG_{ads} (kJ.mol^{-1})	ΔS_{ads} (kJ.mol^{-1}.K^{-1})
AS_3	-7.01183	298	0.9998	9.00935E-05	9524.3872	3.978837	-32.64942868	0.086462
		308	0.9998	7.85574E-05	8565.6849	3.932762	-33.47337734	0.085914
		318	0.9999	2.87776E-05	7906.4188	3.89798	-34.34843139	0.086416
		328	1	2.29749E-05	7341.1642	3.865765	-35.22628935	0.084922
AS_4	-21.2315	298	0.9998	9.6153E-05	14917.185	4.173687	-33.76101209	0.042045
		308	0.9997	0.000128223	10892.412	4.037124	-34.08872235	0.041744
		318	0.9995	0.000273395	8622.0326	3.93561	-34.5775104	0.041969
		328	0.9991	0.000466132	6757.8058	3.829806	-35.00049661	0.041979

Typically, $\Delta G°_{ads}$ values around or near -20 kJ/mol are characteristic of physical adsorption [36], whereas values of -40 kJ/mol or below are generally associated with chemical adsorption. According to this work, the measured $\Delta G°_{ads}$ value suggests a reversible physical adsorption process taking place on a surface with uniform energetic properties. The low value of $\Delta G°_{ads}$ at 328 K, and the presence of a negative sign indicate that the reaction is spontaneous, confirming the adsorption phenomenon and the development of a stable adsorbent film on the steel surface. The adsorption enthalpy $\Delta H°_{ads}$ was determined through the Van't Hoff Eq. (5):

$$\text{Log } K_{ads} = (-\Delta H°_{ads} / 2.303\ RT) + \text{Const} \quad (5)$$

When plotting $\text{Log}K_{ads}$ versus 1/T, a negative linear slope of $-\Delta H°_{ads}/(2.303R)$ is determined, as shown in Figure 11 and Figure 12. Using Eq. (6), the thermodynamic approach allows for the estimate of the adsorption entropy $\Delta S°_{ads}$ for both AS_3 and AS_4.

$$\Delta G°_{ads} = \Delta H°_{ads} - T\Delta S°_{ads} \quad (6)$$

Based on previous studies, a negative $\Delta H°_{ads}$ value indicates that heat is released to the surroundings during adsorption, characterizing the process as exothermic. In contrast, a positive $\Delta H°_{ads}$ value suggests heat absorption from the surrounding medium into the system, reflecting the endothermic behavior of the reaction [37].

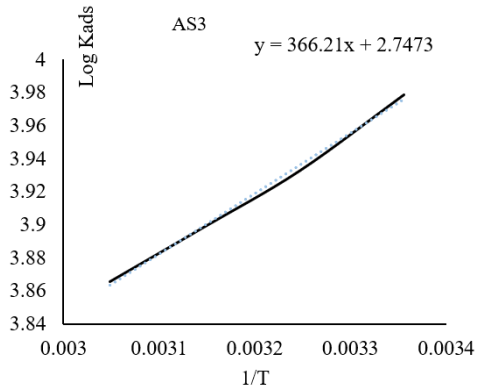

Figure 11. $\text{Log}K_{ads}$ vs.1/T for N80 carbon steel immersed in 1 M HCl at different AS_3 concentrations

The study results indicate that the adsorption of inhibitors is characterized by negative $\Delta H°_{ads}$ data (-7.01183, -24.5022) kJ/mol for the AS_3 and AS_4, in the same order, confirming the exothermic nature of the process is and thus the adsorption can be physical, chemical, or both are expected to occur. Therefore, the large and positive $\Delta S°_{ads}$ value indicates increased disorder when the reactant is converted to the adsorbent, thereby promoting adsorption on the steel surface. In this study, the Langmuir adsorption isotherm was selected due to its excellent agreement with the experimental data ($R^2 \geq 0.99$), maintaining consistency across various temperatures and inhibitor concentrations. This strong linear correlation suggests a monolayer adsorption process on a homogeneous metal surface with negligible inhibitor-inhibitor interactions. While other isotherm models, such as the Freundlich or Temkin, are commonly employed in corrosion inhibition studies, they are typically suited for heterogeneous surfaces where adsorption energy varies with surface coverage-conditions that were not evident in the present system [38]. Attempts to fit the same data using the Freundlich model yielded significantly lower correlation coefficients (R^2 values), indicating a poor fit. Thus, the Langmuir isotherm was identified as the most suitable model to descriptor for the inhibitor-metal interaction in this environment [39].

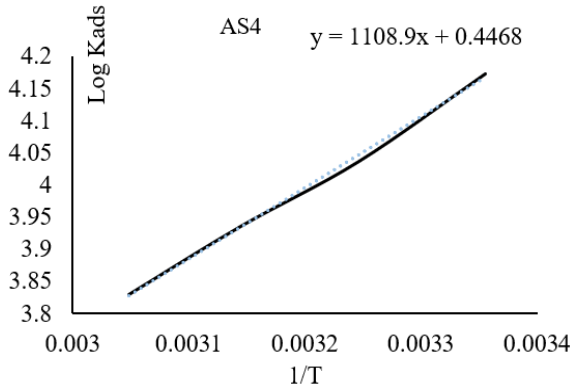

Figure 12. $\text{Log}K_{ads}$ vs.1/T for N80 carbon steel immersed in 1 M HCl at different AS_4 concentrations

3.4 Activation energy (Ea)

The activation energy of both inhibitors was evaluated

Using the Arrhenius Eq. (7) [40, 41], in 1M acidic medium, across varying inhibitor concentration and temperatures.

$$\text{Log icorr} = \text{Log A} - E_a / (2.303RT) \quad (7)$$

The parameters icorr, A, Ea, R, and T denote the corrosion current density the pre-exponential factor (associated with the frequency of molecular collisions of the inhibitor), activation energy, the universal gas constant (R=8.314 J. K^{-1}.mol^{-1}), and absolute temperature in kelvin. when plotting the logarithmic value of (icorr) against the inverse of T, as illustrated in Figure 13 and Figure 14, a linear relationship is observed. The slope of this line corresponds to -Ea/2.303R, while the y-intercept reflects the value of log(A).

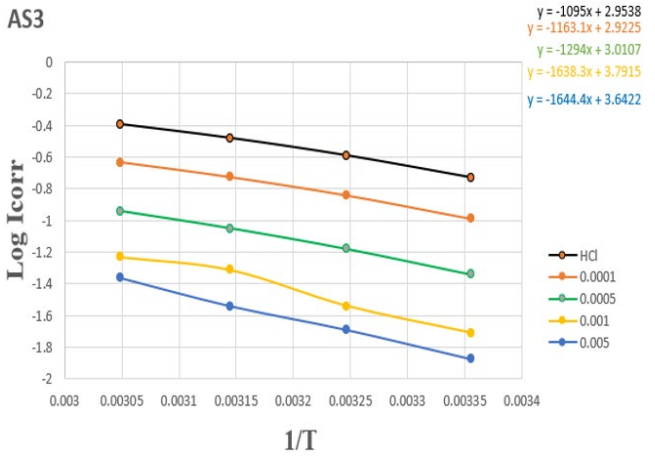

Figure 13. Arrhenius plots for N80 steel with and without AS_3 inhibitor at 298- 328 K

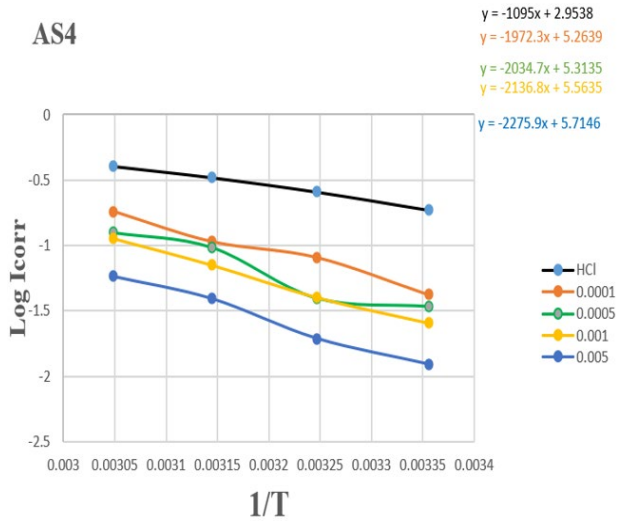

Figure 14. Arrhenius plots for N80 steel with and without AS_4 inhibitor at 298- 328 K

From Table 4, we note that the values of activation energy (Ea) for the corrosion of carbon steel are different when the inhibitor is present compared to its absence, which explains the formation of a layer of inhibitor that is adsorbed on the metal surface and has a physical (electrostatic) nature [42]. This is consistent with the reduction in inhibition performance as temperature rises, suggesting that the initial stage involves physical adsorption, followed by a chemical adsorption process (chemisorption) [43]. The potential for partial chemisorption at elevated temperatures cannot be entirely disregarded. This may stem from the possibility of stronger interactions forming between the inhibitor's functional moieties-such as hydroxyl, methoxy, and amide groups-and the metallic surface, particularly under prolonged exposure. Similar dual-mode adsorption behaviors have been observed in comparable systems, where initial physical adsorption gradually transitions into chemical bonding as the temperature increases. Hence, the mechanism proposed in this study may involve a temperature-dependent shift, where physisorption dominates at mild conditions, while chemisorption becomes increasingly relevant under more aggressive environments [44].

3.5 SEM and EDS analysis [45]

After immersion in 1 M HCl for 180 minutes, the surface of the steel was examined using SEM. Figure 15(a) shows the damaged and roughened surface due to corrosion. In contrast, Figure 15(b) and Figure 15(c) show smooth surfaces for samples treated with AS_3 and AS_4, respectively, confirming the creation of a protective layer. EDS was employed to examine the surface composition. Figures 16(a–c) present the EDS spectra corresponding to the SEM images. In uninhibited samples, high oxygen content indicated corrosion products, while the presence of inhibitors significantly reduced oxygen and corrosion-related elements, further confirming the protective effect of AS_3 and AS_4.

Table 4. Values of activation energy (E_a) and Arrhenius constant (A) for systems with and without inhibitors

Comp.	Conc. (M)	E_a (J. K^{-1}.mol^{-1})	A
HCl	1	20.967	899.00032
AS_3	0.0001	22.269	836.4933423
	0.0005	24.776	1024.844241
	0.001	31.369	32560.50943
	0.005	31.485	4387.021023
AS_4	0.0001	37.764	183609.0421
	0.0005	38.958	39967.57146
	0.001	40.913	366019.3404
	0.005	43.576	518312.1551

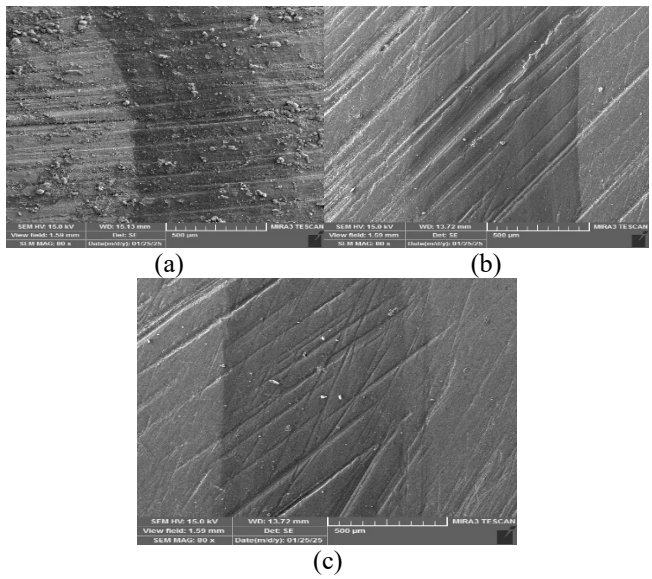

Figure 15. SEM micrographs of the N80 steel surface after treatment with (a) 1 M HCl alone, and (b, c) 1 M HCl containing 0.005 M of AS_3 and AS_4 inhibitors. The scale bars represent 500 µm

The SEM/EDS analysis clearly shows the development of a protective inhibitor coating on the carbon steel surface following immersion in the acidic medium containing AS_3 and AS_4. Although more advanced techniques, such as Atomic Force Microscopy (AFM) or surface profilometry, could have provided deeper insights into the layer's thickness and topography, they were not employed in this study due to instrumentation limitations. Nonetheless, the consistently smoother surface morphology observed in SEM images-combined with the elemental signatures of oxygen, nitrogen, and sulfur identified by EDS-strongly supports the effective adsorption and formation of the protective film. These findings are consistent with previously reported corrosion inhibition mechanisms in which SEM/EDS analyses alone were used to validate surface coverage and inhibitor interaction [45, 46].

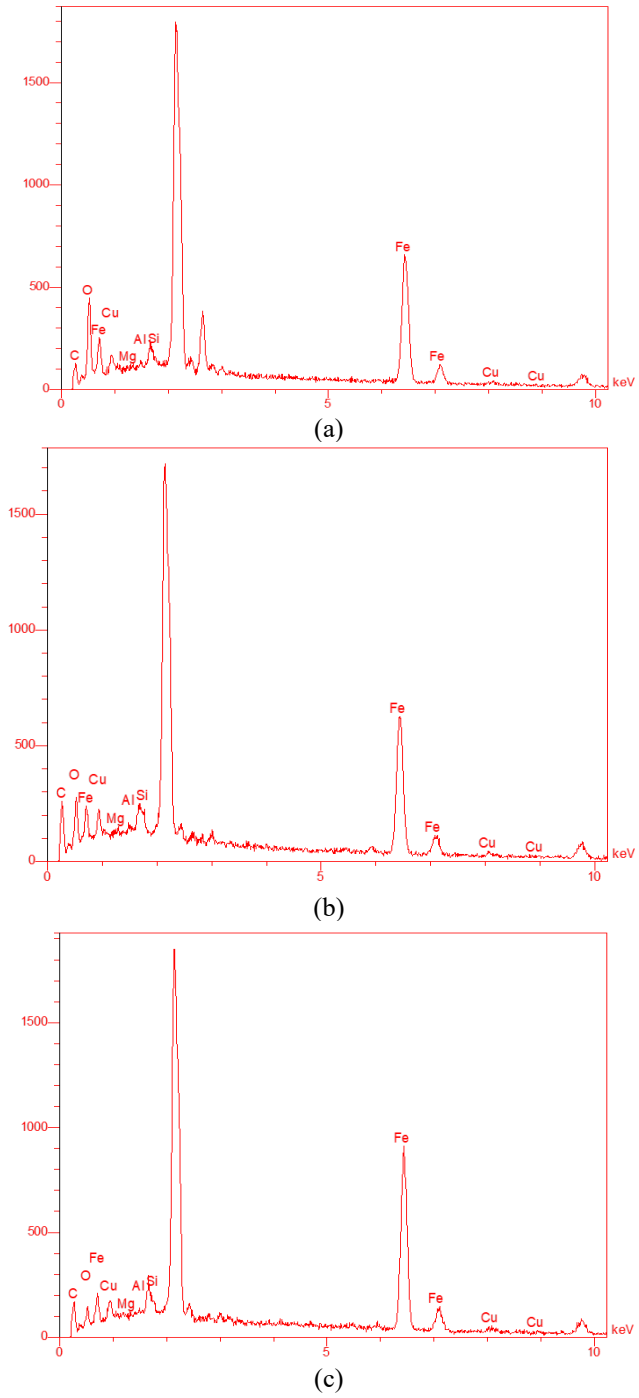

Figure 16. EDX spectra of N80 mild steel after exposure to different solutions (a) 1 M HCl alone, and (b, c) 1 M HCl

3.6 Proposed mechanism of action of inhibitors

Adsorption-type corrosion inhibitors regulate the corrosion process by interfering with the anodic and/or cathodic reaction involved in metal dissolution. The protective effect of organic inhibitors arises primarily from their ability to adsorb onto the metal surface, where they form a barrier film that hinders the interaction between the metal and the corrosive environment [47]. This adsorption mechanism generally combines both physical and chemical interactions, rather than being exclusively one or the other. The adsorption behavior of organic corrosion inhibitors is significantly affected by several factors, including their chemical structure, the nature of the functional groups present, charge distribution in the molecule, the surface charge of the metal, and the characteristics of the corrosive medium, such as PH and electrode potential. Physical adsorption typically arises from electrostatic attraction between oppositely charged inhibitor molecules and the metal surface. In contrast, chemical adsorption involves donor-acceptor interactions, where lone electron pairs from the inhibitor interact with empty low-energy orbitals on the steel surface. As illustrated in Figure 17. Compound AS_4 was chosen to study the inhibition mechanism [48] on the metal surface, as it has a higher inhibition efficiency than other compounds, and this mechanism applies to all other compounds. For organic compounds to function effectively as corrosion inhibitors, they should possess heteroatoms like nitrogen, oxygen, sulfur, and phosphorus, which carry lone electron pairs. Additionally, the presence of π electron systems, such as aromatic rings or conjugated double bonds, enhances their adsorption onto the steel surface by facilitating interaction with the vacant d-orbitals of the steel.

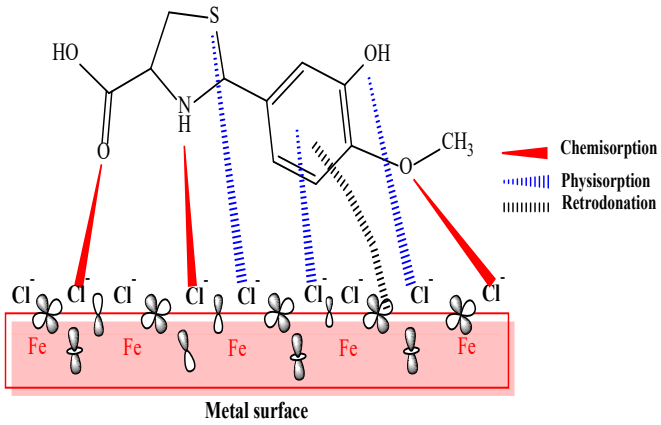

Figure 17. A proposed mechanism for the adsorption of the inhibitor on the metal surface

4. CONCLUSIONS

This study confirmed the corrosion inhibition efficiency of two synthesized thiazolidine derivatives, AS_3 and AS_4, on N80 carbon steel in 1 M HCl medium. The polarization measurements showed that both compounds acted as mixed-type inhibitors. The efficiency increased with higher inhibitor concentrations but decreased with temperature, suggesting physical adsorption. Adsorption studies followed the Langmuir isotherm model with high correlation, indicating monolayer adsorption and spontaneous adsorption mechanisms. SEM and EDS analyses validated the formation

of a protective film on the steel surface in the presence of inhibitors. The promising inhibition efficiency and environmentally benign composition of AS_3 and AS_4 suggest strong potential for deployment across a variety of industrial sectors where acidic corrosion is prevalent. These compounds may serve effectively as protective additives in oil and gas pipeline systems, acidizing treatments in wellbores, chemical processing equipment, and marine coatings exposed to harsh environments. Moreover, their high performance at low concentrations and ease of synthesis underscore their suitability for practical industrial implementation, pending further optimization and on-site validation.

ACKNOWLEDGMENTS

This research is supported by the Department of Chemistry, College of Education of Pure Sciences, University of Basrah, as part of a PhD graduation requirements.

REFERENCES

[1] Zehra, S., Mobin, M., Aslam, J. (2022). An overview of the corrosion chemistry. Environmentally Sustainable Corrosion Inhibitors, 2022: 3-23. https://doi.org/10.1016/B978-0-323-85405-4.00012-4

[2] Basik, M., Mobin, M. (2022). Environmentally sustainable corrosion inhibitors in the oil and gas industry. In Environmentally Sustainable Corrosion Inhibitors, Elsevier, pp. 405-421. https://doi.org/10.1016/B978-0-323-85405-4.00017-3

[3] Belous, A., Tovstolytkin, A., Fedorchuk, O., Shlapa, Y., Solopan, S., Khomenko, B. (2021). Al-doped yttrium iron garnets Y3AlFe4O12: Synthesis and properties. Journal of Alloys and Compounds, 856: 158140. https://doi.org/10.1016/j.jallcom.2020.158140

[4] Jiang, G., Xu, D., Feng, P., Guo, S., Yang, J., Li, Y. (2021). Corrosion of FeCrAl alloys used as fuel cladding in nuclear reactors. Journal of Alloys and Compounds, 869: 159235. https://doi.org/10.17675/2305-6894-2024-13-2-27

[5] Moustafa, A.H., Abdel-Rahman, H.H., Barakat, A., Mohamed, H.A., El-Kholany, A.S. (2024). An exploratory experimental analysis backed by quantum mechanical modeling, spectroscopic, and surface study for C-steel surface in the presence of hydrazone-based Schiff bases to fix corrosion defects in acidic media. ACS Omega, 9(14): 16469-16485. https://doi.org/10.1021/acsomega.4c00199

[6] Kuraimid, Z.K., Abid, D.S., Fouda, A.E.A.S. (2023). Synthesis and characterization of a novel quaternary ammonium salt as a corrosion inhibitor for oil-well acidizing processes. ACS Omega, 8(30): 27079-27091. https://doi.org/10.1021/acsomega.3c02094

[7] Jarallah, H.M., Khadium, M.Y., AbdulNabi, A.S. (2022). Asymmetric azo compounds synthesis, characterization and study them as corrosion inhibitors for carbon steel in acidic medium. Egyptian Journal of Chemistry, 65(8): 57-63.

[8] Jabbar, A., Abdulnabi, A. (2024). Corrosion inhibitors for carbon steel N80 in an acidic medium by using the compound (E)-N-(benzo [d] thiazol-2-yl)-1-(2, 3-dihydrobenzo [b][1, 4] dioxin-6-yl) methanimine. International Journal of Corrosion and Scale Inhibition, 13(2): 1146-1163. https://doi.org/10.17675/2305-6894-2024-13-2-27

[9] Al-Amiery, A.A., Isahak, W.N.R.W., Al-Azzawi, W.K. (2023). Corrosion inhibitors: Natural and synthetic organic inhibitors. Lubricants, 11(4): 174. https://doi.org/10.3390/lubricants11040174

[10] Al-Ashoor, S.Z., Ali, D.S., Al-Sawaad, H.Z. (2023). *Ziziphus spina* Christi leaves methanol extract evaluation as antifungal, antibacterial, antioxidant and green inhibitor for carbon steel alloy corrosion in hydrochloric acid. Portugaliae Electrochimica Acta, 41(2): 167-184. https://doi.org/10.4152/pea.2023410205

[11] Laamari, R., Benzakour, J., Berrekhis, F., Abouelfida, A., Derja, A., Villemin, D. (2011). Corrosion inhibition of carbon steel in hydrochloric acid 0.5 M by hexa methylene diamine tetramethyl-phosphonic acid. Arabian Journal of Chemistry, 4(3): 271-277. https://doi.org/10.1016/j.arabjc.2010.06.046

[12] Masaret, G.S., Shah, R. (2024). Synthesis and evaluation of a novel pyridinyl thiazolidine derivative as an antioxidant and corrosion inhibitor for mild steel in acidic environments. Arabian Journal of Chemistry, 17(6): 105807. https://doi.org/10.1016/j.arabjc.2024.105807

[13] Alamry, K.A., Aslam, R., Khan, A., Hussein, M.A., Tashkandi, N.Y. (2022). Evaluation of corrosion inhibition performance of thiazolidine-2, 4-diones and its amino derivative: Gravimetric, electrochemical, spectroscopic, and surface morphological studies. Process Safety and Environmental Protection, 159: 178-197. https://doi.org/10.1016/j.psep.2021.12.061

[14] Chahir, L., Benzbiria, N., Tahri, F.Z., El Faydy, M., Benhiba, F., et al. (2024). Experimental and theoretical approach for a better understanding of the mechanisms of adsorption and inhibition of corrosion for carbon steel by thiazolidine derivatives in 1 M HCl medium. Physical Chemistry Chemical Physics, 26(36): 23766-23783. https://doi.org/10.1039/d4cp02609h

[15] Qi, W., Huang, Y., Ma, Y., Yu, Z., Zhu, X. (2023). Developing novel imidazoline-modified glucose derivatives as eco-friendly corrosion inhibitors for Q235 steel. RSC Advances, 13(20): 13516-13525. https://doi.org/10.1039/d3ra00222e

[16] Ait Bouabdallah, I., Adjal, F., Zaabar, A., Benchikh, A., Guerniche, D., et al. (2024). Cleome arabica L. extract as a novel green corrosion inhibitor for AISI 1045 carbon steel in 0.5 M HCl: Insights from experimental and theoretical DFT analyses. RSC Advances, 14(49): 36423-36436. https://doi.org/10.1039/d4ra06477a

[17] Verma, C., Chauhan, D.S., Aslam, R., Banerjee, P., Aslam, J., et al. (2024). Principles and theories of green chemistry for corrosion science and engineering: Design and application. Green Chemistry, 26(8): 4270-4357. https://doi.org/10.1039/d3gc05207a

[18] Al-Hujaj, H.H., Majed, A.A., Abdalzahra, Q.R., Abid, D.S., Faisal, N.H., et al. (2025). Thiazolidine derivatives as promising prostate cancer agents: Design, synthesis, in vitro evaluation, DFT, ADME, POM, docking, and toxicity studies. Journal of Molecular Structure, 1340: 142544. https://doi.org/10.1016/j.molstruc.2025.142544

[19] Chen, L., Lu, D., Zhang, Y. (2022). Organic compounds as corrosion inhibitors for carbon steel in HCl solution: A comprehensive review. Materials, 15(6): 2023.

https://doi.org/10.3390/ma15062023
[20] Chandra-Ambhorn, S., Ieamsupapong, S., Thanateponake, V., Suksamai, W. (2009). Effect of coiling temperature on the formation and pickling behaviour of tertiary scale on hot-rolled carbon steel strip. Key Engineering Materials, 410: 669-676. https://doi.org/10.4028/www.scientific.net/KEM.410-411.669
[21] A. Majed, A., Al-Duhaidahawi, D., A. Omran, H., Abbas, S., S. Abid, D., Y. Hmood, A. (2024). Synthesis, molecular docking of new amide thiazolidine derived from isoniazid and studying their biological activity against cancer cells. Journal of Biomolecular Structure and Dynamics, 42(24): 13485-13496. https://doi.org/10.1080/07391102.2023.2276313
[22] Omran, H.A., Majed, A.A., Hussein, K., Abid, D.S., Abdel-Maksoud, et al. (2024). Anti-cancer activity, DFT, and molecular docking study of new bisthiazolidine amide. Results in Chemistry, 12: 101835. https://doi.org/10.1016/j.rechem.2024.101835
[23] Alsayari, A., Muhsinah, A.B., Asiri, Y.I., Al-Aizari, F.A., Kheder, N.A., et al. (2021). Synthesis, characterization, and biological evaluation of some novel pyrazolo [5, 1-b] thiazole derivatives as potential antimicrobial and anticancer agents. Molecules, 26(17): 5383. https://doi.org/10.3390/molecules26175383
[24] Ahmed, S.K., Ali, W.B., Khadom, A.A. (2019). Synthesis and investigations of heterocyclic compounds as corrosion inhibitors for mild steel in hydrochloric acid. International Journal of Industrial Chemistry, 10(2): 159-173. https://doi.org/10.1007/s40090-019-0181-8
[25] Sehmi, A., Ouici, H.B., Guendouzi, A., Ferhat, M., Benali, O., Boudjellal, F.J.J.S. (2020). Corrosion inhibition of mild steel by newly synthesized pyrazole carboxamide derivatives in HCl acid medium: Experimental and theoretical studies. Journal of the Electrochemical Society, 167(15): 155508. https://doi.org/10.1149/1945-7111/abab25
[26] Raviprabha, K., Bhat, R.S. (2023). Corrosion inhibition of mild steel in 0.5 M HCL by substituted 1, 3, 4-oxadiazole. Egyptian Journal of Petroleum, 32(2): 1-10. https://doi.org/10.1016/j.ejpe.2023.03.002
[27] Chaitra, T.K., Mohana, K.N., Tandon, H.C. (2017). Comparative study of Levofloxacin and its amide derivative as efficient water soluble inhibitors for mild steel corrosion in hydrochloric acid solution. International Journal of Industrial Chemistry, 8(1): 1-15. https://doi.org/10.1007/s40090-016-0083-y
[28] Raheema, M.H., Khudhair, N.A., AL-Noor, T.H., Al-Ayash, S.R., Kharnoob, H.H., Obed, S.M. (2023). Enhancement of corrosion protection of metal carbon steel C45 and stainless steel 316 by using inhibitor (Schiff base) in sea water. Baghdad Science Journal, 20(3): 30. https://doi.org/10.21123/bsj.2023.7749
[29] Zhu, Y., Sun, Q., Wang, Y., Tang, J., Wang, Y., Wang, H. (2021). Molecular dynamic simulation and experimental investigation on the synergistic mechanism and synergistic effect of oleic acid imidazoline and l-cysteine corrosion inhibitors. Corrosion Science, 185: 109414. https://doi.org/10.1016/j.corsci.2021.109414
[30] Palumbo, G., Gorny, M., Banaś, J. (2019). Corrosion inhibition of pipeline carbon steel (N80) in CO2-saturated chloride (0.5 M of KCl) solution using gum arabic as a possible environmentally friendly corrosion inhibitor for shale gas industry. Journal of Materials Engineering and Performance, 28(10): 6458-6470. https://doi.org/10.1007/s11665-019-04379-3
[31] Fouda, A.S., Abdallah, M., Atya, A.M., Sabaa, H.D. (2012). Corrosion inhibition of copper in nitric acid solution using some secondary amines. Corrosion, 68(7): 610-619. https://doi.org/10.5006/0454
[32] Palumbo, G., Kollbek, K., Wirecka, R., Bernasik, A., Górny, M. (2020). Effect of CO_2 partial pressure on the corrosion inhibition of N80 carbon steel by gum arabic in a CO2-water saline environment for shale oil and gas industry. Materials, 13(19): 4245. https://doi.org/10.3390/ma13194245
[33] Kokalj, A. (2023). On the use of the Langmuir and other adsorption isotherms in corrosion inhibition. Corrosion Science, 217: 111112. https://doi.org/10.1016/j.corsci.2023.111112
[34] El Hajam, M., Idrissi Kandri, N., Özdemir, S., Plavan, G., Ben Hamadi, N., Boufahja, F., Zerouale, A. (2023). Statistical design and optimization of Cr (VI) adsorption onto native and HNO_3/NaOH activated cedar sawdust using AAS and a response surface methodology (RSM). Molecules, 28(21): 7271. https://doi.org/10.3390/molecules28217271
[35] Khormali, A., Ahmadi, S. (2023). Experimental and modeling analysis on the performance of 2-mercaptobenzimidazole corrosion inhibitor in hydrochloric acid solution during acidizing in the petroleum industry. Journal of Petroleum Exploration and Production Technology, 13(11): 2217-2235. https://doi.org/10.1007/s13202-023-01675-6
[36] Shwetha, K.M., Praveen, B.M., Devendra, B.K. (2024). A review on corrosion inhibitors: Types, mechanisms, electrochemical analysis, corrosion rate and efficiency of corrosion inhibitors on mild steel in an acidic environment. Results in Surfaces and Interfaces, 16: 100258. https://doi.org/10.1016/j.rsurfi.2024.100258
[37] Daoud, D., Douadi, T., Issaadi, S., Chafaa, S. (2014). Adsorption and corrosion inhibition of new synthesized thiophene Schiff base on mild steel X52 in HCl and H2SO4 solutions. Corrosion Science, 79: 50-58. https://doi.org/10.1016/j.corsci.2013.10.025
[38] Vaszilcsin, C.G., Putz, M.V., Kellenberger, A., Dan, M.L. (2023). On the evaluation of metal-corrosion inhibitor interactions by adsorption isotherms. Journal of Molecular Structure, 1286: 135643. https://doi.org/10.1016/j.molstruc.2023.135643
[39] Perumal, S., Muthumanickam, S., Elangovan, A., Muniyappan, N., Kannan, R.S., Krishnamoorthi, K. (2024). Adsorption and corrosion inhibiting behavior of Black Vitex Nigundo leaf extract on mild steel corrosion on 1N HCl and 1N H2SO4. Letters in Applied NanoBioScience, 13(1): 12. https://doi.org/10.33263/LIANBS131.012
[40] Rahiman, A.F.S.A., Sethumanickam, S. (2017). Corrosion inhibition, adsorption and thermodynamic properties of poly (vinyl alcohol-cysteine) in molar HCl. Arabian Journal of Chemistry, 10: S3358-S3366.
[41] Go, L.C., Depan, D., Holmes, W.E., Gallo, A., Knierim, K., Bertrand, T., Hernandez, R. (2020). Kinetic and thermodynamic analyses of the corrosion inhibition of synthetic extracellular polymeric substances. PeerJ Materials Science, 2: e4. https://doi.org/10.7717/peerj-matsci.4

[42] Szauer, T., Brandt, A. (1981). Adsorption of oleates of various amines on iron in acidic solution. Electrochimica Acta, 26(9): 1253-1256. https://doi.org/10.1016/0013-4686(81)85107-9

[43] Douadi, T., Hamani, H., Daoud, D., Al-Noaimi, M., Chafaa, S. (2017). Effect of temperature and hydrodynamic conditions on corrosion inhibition of an azomethine compounds for mild steel in 1 M HCl solution. Journal of the Taiwan Institute of Chemical Engineers, 71: 388-404. https://doi.org/10.1016/j.jtice.2016.11.026

[44] Toghan, A., Alduaij, O.K., Fawzy, A., Mostafa, A.M., Eldesoky, A.M., Farag, A.A. (2024). Effect of adsorption and interactions of new triazole-thione-schiff bases on the corrosion rate of carbon steel in 1 M HCl solution: Theoretical and experimental evaluation. ACS Omega, 9(6): 6761-6772. https://doi.org/10.1021/acsomega.3c08127

[45] Al-Moubaraki, A.H., Obot, I.B. (2021). Top of the line corrosion: Causes, mechanisms, and mitigation using corrosion inhibitors. Arabian Journal of Chemistry, 14(5): 103116. https://doi.org/10.1016/j.arabjc.2021.103116

[46] Yan, X., Zhao, M., Yan, R., Wang, X., Dai, C. (2023). Statistical analysis of gelation mechanism of high-temperature CO2-responsive smart gel system. Journal of Molecular Liquids, 377: 121521. https://doi.org/10.1016/j.molliq.2023.121521

[47] Alamry, K.A., Hussein, M.A., Musa, A., Haruna, K., Saleh, T.A. (2021). The inhibition performance of a novel benzenesulfonamide-based benzoxazine compound in the corrosion of X60 carbon steel in an acidizing environment. RSC Advances, 11(12): 7078-7095. https://doi.org/10.1039/d0ra10317a

[48] Oguzie, E.E., Li, Y., Wang, S.G., Wang, F. (2011). Understanding corrosion inhibition mechanisms—Experimental and theoretical approach. RSC Advances, 1(5): 866-873. https://doi.org/10.1039/C1RA00148E